Molecular Description of Erosion Phenomena in Biodegradable Polymers

Matt J. Kipper and Balaji Narasimhan*

Department of Chemical Engineering, Iowa State University, 2114 Sweeney Hall, Ames, Iowa 50011-2230

Received November 13, 2004; Revised Manuscript Received December 13, 2004

ABSTRACT: A new model for the erosion kinetics of semicrystalline surface-erodible homopolymers and copolymers is presented. The model is derived for a class of surface-erodible polyanhydride copolymers, with the goal of describing erosion in terms of fundamental, elementary processes. This model is based on an accurate description of copolymer microstructure and can thereby account for the heterogeneous erosion due to microphase separation and crystallinity. In addition to accurately predicting the overall erosion profile and the release of individual monomer species, several key phenomena that occur during erosion are described. These include precipitation of slightly soluble degradation products inside the pores of the erosion zone and pH changes during erosion due to dissolution of acidic monomers and the consequent changes in monomer solubility. This model also motivates future experiments to investigate predicted phenomena such as the effects due to local changes in pH and degradation rate constants for crystalline and amorphous moieties. The rational design of biomedical devices such as vehicles for drug delivery and scaffolds for tissue engineering will be aided by the application of this model and future extensions of it.

Introduction

Bioerodible polymers are ideal for a variety of biomedical applications. Their chemistries can be tailored to stabilize macromolecular drugs,[1] their surfaces can be modified to target delivery to specific cells and tissues,[2] and their erosion kinetics can be modulated by a variety of techniques.[3−9] Bioerodible polymers have been used to fabricate scaffolds for tissue engineering,[10,11] implants for orthopedic applications,[12] and vehicles for targeted and controlled drug delivery.[13−18] In all of these applications, the erosion kinetics is key to the performance of the device. The erosion kinetics can be modulated by altering copolymer composition when the two constituent polymers erode at different rates or by changing the crystallinity when crystalline and amorphous domains erode at different rates.

Surface-eroding polymers, such as polyanhydrides and poly(ortho esters), are a particularly promising class of bioerodible polymers for many biomedical applications. They do not swell in the presence of water. Rather, their hydrophobicity prevents the ingress of water. This hydrophobic environment may be advantageous for stabilizing macromolecular drugs such as proteins, growth hormones, and vaccines.[19] For controlled-release applications, drug release kinetics is controlled by the erosion kinetics, rather than by swelling and diffusion as in some bulk-eroding systems.[20] Since the eroding zone is limited to the surface, the bulk polymer maintains its shape and mechanical integrity as the device shrinks, which may be desirable for orthopedic applications.

However, the erosion kinetics is complicated when phases or components are added, as in the case of semicrystalline polymers or microphase-separated copolymers. When the two phases erode at different rates, surface-eroding polymers begin to exhibit some characteristics of bulk-eroding polymers. The erosion of a fast eroding phase may leave behind a porous microstructure of the slow eroding phase. Water may then penetrate into the eroding zone, drugs may diffuse out of the material, and the mechanical properties in the eroding zone are subject to significant change. The rational design of biomedical devices based on surface-eroding phase-separated polymers requires a detailed understanding of the mechanisms of erosion that lead to these phenomena.

Several approaches to understand and model the erosion mechanisms of surface-erodible polymers have appeared in the literature. Thombre and Himmelstein have developed a phenomenological model in which the erosion front progresses through the device while diffusion is permitted in the intact zone.[21] A diffusion barrier representing an external membrane is added. An extension of this model accounts for diffusion of the degradation products and for catalyzed polymer degradation.[22] Zygourakis proposed a cellular automata approach in which individual volume elements are assigned erosion times upon exposure to water. A porous microstructure develops as the polymer erodes.[23,24] Göpferich and Langer have proposed a similar model.[25] In their model, each volume element erodes stochastically and an extension of the model accounts for monomer diffusion through the porous erosion zone.[26] Batycky et al. developed a mechanistic model that explicitly accounts for polymer degradation by both random chain scission and end chain scission rather than simply modeling erosion as an elementary process.[27] Drug release is also accounted for by desorption from the polymer matrix and by diffusion through mesopores. A nonhomogeneous distribution of drug is accounted for in a drug-release model proposed by Varelas et al., but the polymer matrix does not erode.[28,29]

* Author to whom correspondence should be addressed. Tel: (515) 294-8019. Fax: (515) 294-2689. E-mail: nbalaji@iastate.edu.

10.1021/ma047661r CCC: $30.25
Published on Web 01/29/2005

In this model, isolated domains act as reservoirs from which drug diffuses through a polymer matrix. We have developed a model for erosion and drug release that accounts for microphase-separated domains that erode at different rates and for partitioning of encapsulated drugs within the phase-separated domains.[30] However, our previous model assumes that erosion is primarily controlled by degradation and ignores the subsequent mass-transfer phenomena of dissolution and diffusion.

Experimentally Observed Features of Polyanhydride Erosion

Most polyanhydride copolymers that have been synthesized for biomedical applications are semicrystalline.[31] It has been demonstrated experimentally that the amorphous phase of semicrystalline polyanhydrides erodes faster than the crystalline phase.[32−34] In most cases, the spherulitic structure of the crystalline phase remains somewhat intact as the amorphous phase degrades, leaving behind a porous matrix, the morphology of which is defined by the original morphology of the crystalline/amorphous phase separation.

The erosion mechanism of semicrystalline, surface-erodible copolymers is complex and consists of several elementary steps, beginning with degradation. In the case of binary A−B copolymers, three types of bonds are available for degradation: A−A bonds, A−B bonds, and B−B bonds. It has been shown that for copolymers of sebacic anhydride (SA) and 1,3-bis(*p*-carboxyphenoxy)-propane (CPP) the SA−SA bonds and SA−CPP bonds are hydrolyzed at a faster rate than the CPP−CPP bonds.[35,36] This also leads to the observed heterogeneous release of degraded monomer from these copolymer systems.[37,38]

In addition to the reactivity of the anhydride bonds, the monomer solubility may also affect polyanhydride erosion kinetics. Göpferich et al. have demonstrated the precipitation of monomers inside the eroding zone of CPP−SA copolymers[39] and fatty acid dimer−SA (FAD−SA) copolymers.[40] This phenomenon occurs because anhydride bonds in the polymer backbone degrade, resulting in monomer formation at a rate faster than the rate of monomer dissolution. As the solution inside the porous eroding zone of the polymer approaches saturation, monomer crystals accumulate. Closely coupled to the precipitation and dissolution of the monomers is their effect on the pH of the microenvironment inside the eroding polymer matrix. This pH has been successfully measured in 20:80 CPP−SA copolymer tablets by Mäder et al. using spectral spatial electron paramagnetic resonance imaging (EPRI).[41] They detected pH levels as low as 4.7 in the eroding zone, which rose as the polymer continued to erode and the monomer diffused from the device. The decrease in pH further limits the monomer solubility, as the dicarboxylic acid monomers become much less soluble at low pH.[39]

The decrease in pH inside the eroding zone may not have a strong effect on the degradation kinetics; the degradation of polyanhydrides is known to be base catalyzed.[42,43] However, the dissolution kinetics and solubility of the dicarboxylic acid monomers is most likely affected by pH.

Our goal in this paper is to understand the mechanism of polymer erosion at a molecular level and to accurately describe the erosion kinetics of surface-eroding phase-separated copolymers. This work is also motivated by our previous experiments with polyanhydride copolymers composed of 1,6-bis(*p*-carboxyphenoxy)hexane (CPH) and SA[13,38,44−47] and on the body of experimental and theoretical work describing this and similar copolymer systems. We would like to point out that this model can be generalized to other surface-eroding systems such as poly(ortho esters) and could be modified to describe bulk-eroding systems (such as poly(lactide-*co*-glycolide) copolymers). Additionally, some of our model predictions motivate additional experiments to measure the effects of various phenomena.

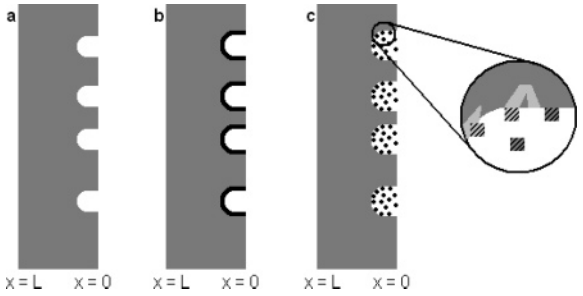

Figure 1. Schematic illustrating erosion process of a tablet with half-thickness *L*, exposed to buffer on the right.

Model Development

Polymer erosion (i.e., mass loss) is the sum of several elementary processes: (1) polymer degradation (monomer formation), (2) monomer, oligomer, and polymer dissolution, and (3) diffusion of dissolved species from the eroded zone

Our view of this complex erosion process is shown in Figure 1. This figure shows a tablet of half-thickness, *L*, exposed to water on the right at three stages during erosion.

We model step one, monomer formation, as a first order process with respect to the surface area of exposed polymer. The exposed polymer surface area is converted to undissolved monomer. Monomer formed in step one is assumed to be in the form of a monolayer, crystallized on the surface, and prevents the underlying polymer from degrading. For the case of the polyanhydrides of interest in this work, we assume that only the monomers are soluble. Figure 1a shows four pores that have formed at the exposed surface of a polymer tablet. Figure 1b shows the monolayer of undissolved monomer (thick solid line). In this model, the monomer formation rate is assumed to be independent of polymer molecular weight, as it has been demonstrated experimentally that polyanhydride erosion rates are not significantly affected by polymer molecular weight.[48] Step two, monomer dissolution, results in mass loss from the device. While undissolved monomer on the surface serves to protect the underlying polymer from degradation, as monomer dissolves, it exposes undegraded polymer. Dissolved monomer is represented in Figure 1c by the particles inside the pores. Some particles remain undissolved, adsorbed to the surface of the pores. A distinction is made between monomer formed from crystalline polymer and monomer formed from amorphous polymer. Probabilities are assigned for the exposure of amorphous polymer and crystalline polymer as the monomer from each of these phases dissolves. This is illustrated in the inset in Figure 1c. Here, the two polymer phases are represented by the light gray and the dark gray regions.

Table 1. Dimensionless Model Variables

variable	definition
f_{ma1}	surface area fraction of monomer formed from amorphous polymer of type one
f_{ma2}	surface area fraction of monomer formed from amorphous polymer of type two
f_{mc1}	surface area fraction of monomer formed from crystalline polymer of type one
f_{mc2}	surface area fraction of monomer formed from crystalline polymer of type two
κ_1	dissolution rate for monomer one
κ_2	dissolution rate monomer two
f_{a1}	surface area fraction of amorphous polymer of type one
f_{a2}	surface area fraction of amorphous polymer of type two
f_{c1}	surface area fraction of crystalline polymer of type one
f_{c2}	surface area fraction of crystalline polymer of type two
R^*	average pore radius
ϵ	porosity
χ_1	concentration of dissolved monomer of type one
χ_2	concentration of dissolved monomer of type two
σ	specific surface area
p_{aa}	probability of amorphous monomer dissolving to expose amorphous polymer
p_{ca}	probability of crystalline monomer dissolving to expose amorphous polymer
ϕ_{a1}	fraction of the amorphous polymer represented by polymer one
ϕ_{c1}	fraction of the crystalline polymer represented by polymer one

Table 2. Dimensionless Model Parameters

parameter	definition
β	ratio of degradation rate constants for crystalline polymer of type one to that for amorphous polymer of type one
γ	ratio of degradation rate constants for amorphous polymer of type two to that for amorphous polymer of type one
δ	ratio of degradation rate constants for crystalline polymer of type two to that for amorphous polymer of type one
λ	long period of crystalline lamellae
D_1^*	diffusion coefficient for monomer of type one
D_2^*	diffusion coefficient for monomer of type two
ξ	distance from the surface
τ	time
α	degree of crystallinity
k_{d1}	dissolution rate constant for monomer of type one
k_{d2}	dissolution rate constant for monomer of type two

The monomers formed from these two phases are represented by the striped blocks. The probability that light gray monomer will dissolve to expose light gray polymer is greater than the probability that light gray monomer will dissolve to expose dark gray polymer. For copolymers, the microphase separation can be accounted for in a similar way. In step three, the monomer diffuses out of the eroding zone in response to the concentration gradient formed in step two. Surface area fractions of each type of monomer and each type of polymer are functions of both position and time. Likewise, the pore radius, porosity, specific surface area, and concentration of dissolved monomer are also functions of position and time.

As monomer dissolves, the pH of the solution inside the eroding zone changes, which alters the dissolution kinetics by changing the saturation concentration. We assume no pH dependence of the degradation kinetics, as we anticipate only acidic conditions in the eroding zone. This is consistent with experimental observations for polyanhydrides[43] but could be modified for acid-catalyzed degradation, as is the case for poly(ortho esters). Dimensionless model variables and parameters are listed in Tables 1 and 2, respectively.

The surface of the pores is characterized by the fractional coverage of amorphous polymer of components one and two, f_{a1} and f_{a2}, crystalline polymer of components one and two, f_{c1} and f_{c2}, and monomer arising from the degradation of each type of polymer, f_{ma1}, f_{ma2}, f_{mc1}, and f_{mc2}. Equations 1−4 determine the surface area fraction of each type of monomer on the surface of a pore. These equations are first order in the surface area fraction of polymer and pseudo-first order in the surface area fraction of monomer since the dimensionless dissolution rates, κ_1 and κ_2, are functions of concentration.

$$\frac{\partial f_{ma1}}{\partial \tau} = f_{a1} - f_{ma1}\kappa_1 \tag{1}$$

$$\frac{\partial f_{ma2}}{\partial \tau} = \gamma f_{a2} - f_{ma2}\kappa_2 \tag{2}$$

$$\frac{\partial f_{mc1}}{\partial \tau} = \beta f_{c1} - f_{mc1}\kappa_1 \tag{3}$$

$$\frac{\partial f_{mc2}}{\partial \tau} = \delta f_{c2} - f_{mc2}\kappa_2 \tag{4}$$

It is necessary to distinguish between the four types of monomer because, as monomer dissolves, it exposes undegraded polymer, as mentioned earlier and illustrated in the inset of Figure 1c. The ratio of the degradation rate constant for the crystalline polymer of type one to that for amorphous polymer of type one is β. The degradation rate constants for amorphous polymer of type two and crystalline polymer of type two are normalized similarly to form the ratios γ and δ, respectively. The dimensionless time parameter, τ, is normalized by the degradation rate constant for amorphous polymer of type one.

$$\tau = \frac{k_{a1}t}{\rho y} \tag{5}$$

Here, t is time (s), k_{a1} is the degradation rate constant for amorphous polymer of type one (g cm^{-2} s^{-1}), ρ is the

density of the polymer (g cm^{-3}), and y is the characteristic length scale (cm) associated with a monolayer of monomer.

Equations 6−9 determine the surface area fraction of each type of polymer. The first term on the right-hand side of each of these equations accounts for polymer degradation, and the second term accounts for exposure of the undegraded polymer as monomer dissolves.

$$\frac{\partial f_{a1}}{\partial \tau} = -f_{a1} + [(p_{aa}f_{ma1} + p_{ca}f_{mc1})\kappa_1 + (p_{aa}f_{ma2} + p_{ca}f_{mc2})\kappa_2]\phi_{a1} \quad (6)$$

$$\frac{\partial f_{a2}}{\partial \tau} = -\gamma f_{a2} + [(p_{aa}f_{ma1} + p_{ca}f_{mc1})\kappa_1 + (p_{aa}f_{ma2} + p_{ca}f_{mc2})\kappa_2](1 - \phi_{a1}) \quad (7)$$

$$\frac{\partial f_{c1}}{\partial \tau} = -\beta f_{c1} + \{[(1 - p_{aa})f_{ma1} + (1 - p_{ca})f_{mc1}]\kappa_1 + [(1 - p_{aa})f_{ma2} + (1 - p_{ca})f_{mc2}]\kappa_2\}\phi_{c1} \quad (8)$$

$$\frac{\partial f_{c2}}{\partial \tau} = -\delta f_{c2} + \{[(1 - p_{aa})f_{ma1} + (1 - p_{ca})f_{mc1}]\kappa_1 + [(1 - p_{aa})f_{ma2} + (1 - p_{ca})f_{mc2}]\kappa_2\}(1 - \phi_{c1}) \quad (9)$$

The probability that monomer from amorphous polymer will expose amorphous polymer upon dissolution is p_{aa}, and the probability that crystalline polymer will expose amorphous polymer is p_{ca}.. The estimation of these probabilities is based on the degree of crystallinity, α, and the microstructure. Appendix A.1 describes how these parameters are estimated on the basis of a balance of the total interfacial area initially present. The chemical identity of the monomer is also important since the two types of monomers dissolve at different rates. The fraction of component one in the amorphous and crystalline phases are ϕ_{a1} and ϕ_{c1}, respectively.

The average dimensionless radius of a pore, R^*, changes as monomer dissolves (see Figure 1b and 1c).

$$\frac{\partial R^*}{\partial \tau} = (f_{ma1} + f_{mc1})\kappa_1 + (f_{ma2} + f_{mc2})\kappa_2 \quad (10)$$

The porosity, ϵ, is the fraction of the total volume that is represented by pores. The pore volume is computed assuming cylindrical pores of average dimensionless radius, R^*. The number of pores is the initial number of amorphous domains, found by dividing the total volume by the volume associated with a long period for the crystalline lamellae. It is assumed that pores eventually overlap and coalesce. This is accounted for by multiplying the pore volume by the total polymer volume. Thus, as the porosity increases, the probability that a pore will intersect another pore increases. Multiplying by the polymer volume prevents counting the volume of the overlap more than once, via a mean field approximation on the porosity distribution.

$$\frac{\partial \epsilon}{\partial \tau} = \frac{8(1 - \epsilon)R^*}{\lambda^2}\frac{\partial R^*}{\partial \tau} \quad (11)$$

Here, λ is the dimensionless long period of the crystalline lamellae and is used to estimate the number of pores.

The dimensionless concentrations of monomer of type one and two, χ_1 and χ_2, in the erosion zone are given by a diffusion equation with a source term for dissolution from the surfaces of the pores.

$$\frac{\partial \chi_1}{\partial \tau} = \frac{(f_{ma1} + f_{mc1})\kappa_1\sigma}{\epsilon} + D_1^*\frac{\partial^2 \chi_1}{\partial \xi^2} \quad (12)$$

$$\frac{\partial \chi_2}{\partial \tau} = \frac{(f_{ma2} + f_{mc2})\kappa_2\sigma}{\epsilon} + D_2^*\frac{\partial^2 \chi_2}{\partial \xi^2} \quad (13)$$

Here, ξ is the dimensionless position from the original surface of the eroding polymer. D_1^* and D_2^* are the dimensionless diffusivities of monomers one and two, respectively. Diffusion only in the direction of propagation of the erosion front is considered. In other words, perfect mixing is assumed in the radial direction inside the pores. Both concentrations are assumed to be zero outside the pores. The dimensionless surface area per unit volume, σ, is computed by assuming cylindrical pores and accounting for coalescence of the pores.

$$\sigma = \frac{2\epsilon(1 - \epsilon)}{R^*} \quad (14)$$

The dimensionless parameters ξ, R^*, D^*, and χ_n, are

$$\xi = \frac{x}{y} \quad (15)$$

$$R^* = \frac{R}{y} \quad (16)$$

$$D_n^* = \frac{D_n\rho}{k_{a1}y} \quad (17)$$

$$\chi_n = \frac{c_n}{\rho} \quad (18)$$

Here, x is the distance from the original surface of the polymer, R is the pore radius, D_n is the diffusivity of the dissolved monomer of type n, and c_n is the concentration of dissolved monomer of type n. The specific surface area, s, and the long period, l, are also normalized by the length scale y to give the parameters σ and λ, respectively.

$$\sigma = sy \quad (19)$$

$$\lambda = \frac{l}{y} \quad (20)$$

The dimensionless dissolution rate for each of the monomers is computed as shown below.

$$\kappa_n = \frac{k_{dn}(c_{sat,n} - c_n)}{c_{sat,n}k_{a1}} \quad (21)$$

Here, c_n and $c_{sat,n}$ are the concentration of dissolved monomer of type n and the concentration of dissolved monomer at saturation of monomer type n, respectively, and k_{dn} is the dissolution rate constant for monomer of type n.

Initial values for the porosity, pore radius, and surface area fractions are all set to zero, with the exception of the surface area fractions of amorphous polymer of types one and two, which are initialized in accordance with the copolymer composition. This assumes that the

amorphous polymer preferentially partitions to the surface.[33,34] Two additional variables, ξ_{ef} and ξ_s, are the respective positions of the erosion front and the surface. Both of these parameters are initially set to zero, and the erosion front moves through the polymer at the same velocity with which the pores radius grows at the erosion front.

$$\frac{\partial \xi_{ef}}{\partial \tau} = \left.\frac{\partial R^*}{\partial \tau}\right|_{\xi = \xi_{ef}} \tag{22}$$

The position of the surface is taken as the lowest value of ξ for which the porosity is less than 1. At ξ_{ef}, an additional source term is added to eqs 12 and 13 to account for the dissolution occurring at the surface normal to the direction of propagation of the erosion front. The cumulative fractional mass loss can be computed by integrating the porosity at any time point.

$$\frac{m(\tau)}{m_\infty} = \int_0^{\xi_{max}} \epsilon(\tau,\xi) d\xi \tag{23}$$

Here, m_∞ is the total mass of the polymer. The cumulative mass loss for each type of polymer is computed by integrating the dissolution rate for the corresponding monomer.

The remaining equations have nonlinearities that suggest a modified finite difference solution. The Crank−Nicolson method is used to formulate finite difference equations (FDEs). Thus, solutions to eqs 1−4 and 6−13 are obtained implicitly with the exception of the parameters κ_1, κ_2, ϕ_1, ϕ_2, p_{aa}, and p_{ca}.. These parameters are computed from the previous time step. Since the equations are stiff, depending on the values of the parameters β, γ, δ, k_{d1}, and k_{d2}, the second-order Gear method is used to integrate the FDEs.[49]

Model Parametrization

Each of the elementary processes listed at the beginning of the previous section that constitute the erosion process has an associated rate constant. The relationships between these rate constants will ultimately determine the nature of the erosion process. Overall, erosion rate constants have been reported for several polyanhydrides, including copolymers.[31] Diffusion coefficients have been reported for the SA and CPP monomers.[26] Dissolution rate constants for dicarboxylic acid monomers, however, are not reported in the literature. To obtain the dissolution rate constants, 10 mm diameter, 100 mg tablets of CPH and SA were melt-pressed using a Carver Press (Wabash, IN) at 3 metric tons for 5 min just above the melting point of the dicarboxylic acid. Tablets were weighed and allowed to dissolve in 900 mL of 0.1 M phosphate buffer (pH 7.4) at 37 °C. The dissolution medium was stirred at 100 rpm. Dissolution experiments were conducted in an SR8-Plus Dissolution Test Station (Hansen Research Inc., Chatsworth, CA). The tablets were removed at specified intervals and dried under vacuum for 24 h. The masses of the tablets were recorded at each of at least 10 time points for each monomer, and the experiments were performed in duplicate. Dissolution rate constants are reported in Table 3. The saturation concentration at different pH values for each dicarboxylic acid was determined by adding excess dicarboxylic acid to 10 mL of 0.1 M phosphate or acetate buffer. Vials were incubated at 37 °C for 2 days with gentle agitation. Concentrations were determined by UV absorbance at 202 nm for SA and 249 nm for CPH.[38] The saturation concentration as a function of pH is shown in Figure 2. The data for CPP and some of the data points for SA are taken from from Göpferich and Langer.[39] The pK_a values for the diacids can be estimated by the positions of the inflection points. These values are also reported in Table 3.

Table 3. Physical Constants for the Dicarboxylic Acids

dicarboxylic acid monomer	dissolution rate constant (g cm^{-2} s^{-1})	pK_{a1}	pK_{a2}
SA	1.4×10^{-6}	4.8	5.6
CPP		4.5[a]	7.9[a]
CPH	1.4×10^{-8}	3.7	6.7

[a] These data are taken from the experiments reported by Göpferich and Langer.[39]

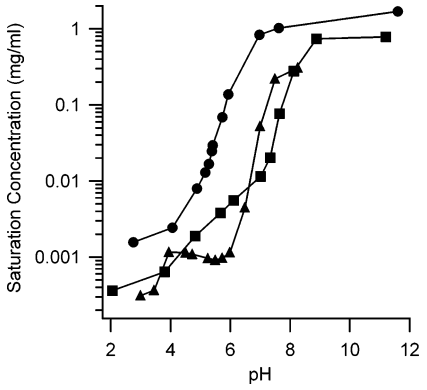

Figure 2. Saturation concentrations of SA (●), CPP (■), and CPH (▲) as a function of pH. CPP data and some data points for SA taken from Göpferich and Langer.[39]

Table 4. Parameters Used to Model Poly(SA) Erosion Kinetics

parameter	value
k_{a1}	8.0×10^{-7} (g cm^{-2} s^{-1})
ρ	1.05 (g cm^{-3})
k_{d1}	1.4×10^{-6} (cm s^{-1})
D_1	6.8×10^{-6} (cm^2 s^{-1})
β	0.001
λ	2.8×10^{-6} (cm)
α	0.6
y	1.0 (nm)

The data in Figure 2 indicate that the saturation concentration for SA is an order of magnitude greater than that for CPP and CPH over the pH range from 5.0 to 7.5. Thus, it is likely that the SA concentration dominates the pH, and hence, the pH inside the eroding zone can be estimated by considering only the SA concentration. If the dissociation of the two carboxylic acids on the SA monomer is considered along with the dissociation of water, a quartic equation for the hydrogen concentration as a function of SA monomer concentration results. The solution of this equation is presented in Appendix A.2. The results in Appendix A.2 demonstrate that a pH below ~4.75 is not obtainable because the concentration of SA required to obtain that pH is above the saturation concentration. This is in good agreement with the experimental findings of Mäder et al. noted earlier.[41] They observed a pH of about 4.7 inside the eroding zone of SA containing copolymers, which would indicate saturation of the erosion zone.

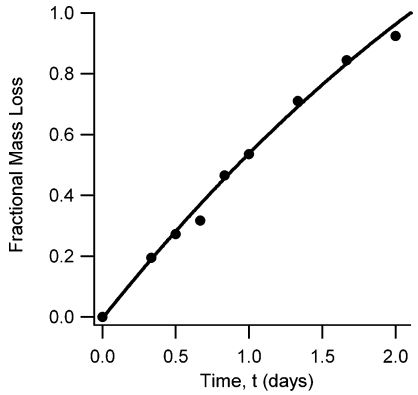

Figure 3. Cumulative fractional mass loss for poly(SA) erosion from experiment[38] (●) and model (line).

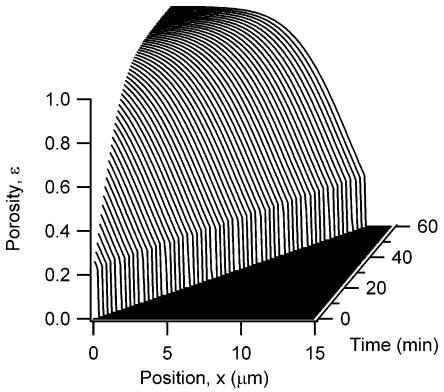

Figure 4. Model results for porosity evolution in the first 60 min of erosion for poly(SA).

Model Solution for Poly(SA)

We first investigate the case of semicrystalline poly(SA) homopolymer erosion. For homopolymers, eqs 2, 4, 7, 9, and 13 are unnecessary and eqs 6, 8, and 10 are simplified by the absence of the terms related to component two. Values of additional parameters are listed in Table 4. The parameters k_{a1} and β were used to fit the model to experimental data for erosion of poly(SA) tablets.[38] The values for λ and α were taken from our previous characterization of the crystallinity.[46]

The model was solved with a time step of 0.05 s and a position step of 1 nm. Several reports of experimental results for erosion of poly(SA) are found in the literature.[38,39,48] We compare our model to the experimental results we have previously obtained.[38] In these experiments, 110 mg tablets, 10 mm in diameter and 1.3 mm in thickness, were degraded in 900 mL of pH 7.4 phosphate buffer at 37 °C with agitation at 100 rpm. The cumulative fractional mass loss as a function of time is plotted in Figure 3 for the experiment and the model.

In addition to accurately describing the overall erosion profile, the new model offers a detailed description of the erosion process. Of particular interest are the microstructural characteristics that can be obtained, including the ratio of the crystalline to amorphous polymer remaining in the erosion zone, the porosity, and the pH in the erosion zone. Figure 4 shows the evolution of the porosity for the first hour of erosion. During the first hour, the erosion front moves 13 μm into the tablet, and the porosity at the surface does not go to 1 until 51 min after the erosion begins. By this time, the erosion front has moved ~11 μm into the tablet. Once the porosity at $x = 0$ reaches unity, the surface begins to move. At this point, a pseudo-steady-state develops with the positions of the surface and the erosion front moving at the same velocity. The erosion zone at any time consists of the region between the surface, $x = x_s$, and the position of the erosion front, $x = x_{ef}$. Since there is a pseudo-steady-state, the thickness of this zone remains constant at ~11 μm until the erosion front reaches the center of the tablet, $x = x_{max}$. Note that initially the porosity increases rapidly as the amorphous polymer erodes, leaving behind a network rich in crystalline domains. The progress of erosion at a given position continues to decelerate as the porosity approaches unity.

The surface area fractions of crystalline polymer, amorphous polymer, and monomer are plotted in Figure 5. Figure 5a shows the surface area fractions (at a given position) as a function of the time after the erosion front passes. Figure 5b shows the surface area fractions (at a given time) as a function of position from the erosion front. Figure 5a demonstrates that within about 90 s of the erosion front passing through a point, the surface area fractions have reached a steady state and the exposed surface area is dominated by crystalline polymer. The two types of monomer and the amorphous polymer together make up about 0.1% of the total surface area. Figure 5b shows that, at a given time, the surface area fractions vary over a relatively narrow distance from the position of the erosion front.

The concentration of SA diacid and the resulting pH in the erosion zone after the pseudo-steady-state devel-

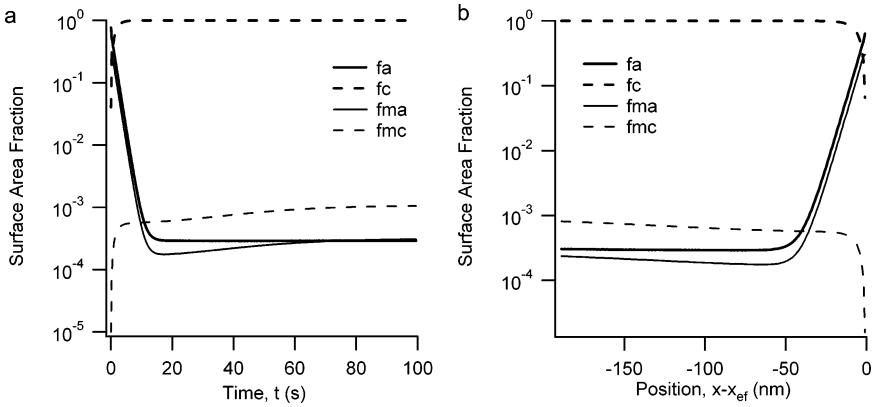

Figure 5. Surface area fractions as a function of time at constant position (a) just after the erosion front passes by and as a function of position at constant time (b) near the erosion front.

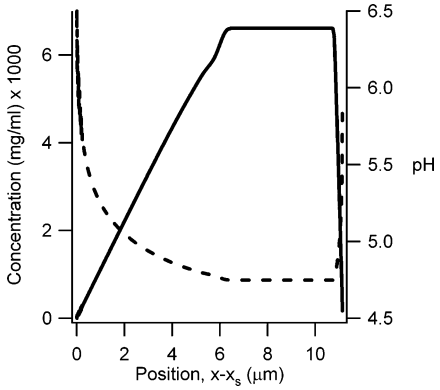

Figure 6. SA concentration (solid line) and the resultant pH (broken line) in the erosion zone.

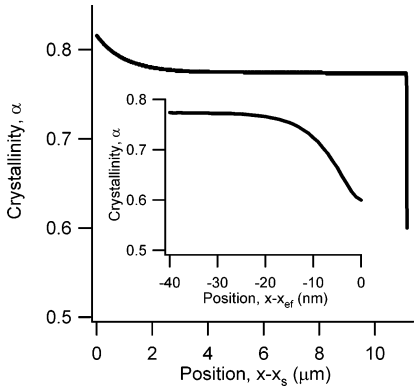

Figure 7. Crystallinity, α, as a function of position at a constant time near the erosion front.

ops is shown as a function of position in Figure 6. The concentration reaches the saturation concentration at ~6 μm from the surface. The pH prediction is in good agreement with the experimental results of Mäder et al.[41]

Although the pore surface within the erosion zone is overwhelmingly dominated by crystalline polymer, a significant fraction of amorphous polymer remains in the bulk throughout the erosion process. This is evident from the plot shown in Figure 7. Here, the crystallinity, α, is plotted as a function of distance from the erosion front. At the erosion front, the crystallinity is 0.6 (the value in the bulk), and just past the erosion front, the crystallinity rises sharply to a value of 0.77 inside the erosion zone (inset). Closer to the surface, the crystallinity rises gradually to about 0.82. The region near the erosion front is shown in the inset.

The crystallinity plot shown in Figure 7 compares well with the experimental results reported in several studies, which indicate that the crystallinity inside the erosion zone is increased over that in the bulk, uneroded polymer.[32−34]

Model Solution for Poly(CPH) and Poly(CPP)

The model was also solved for semicrystalline poly(CPH) and poly(CPP). We chose to model these two chemistries because they have been studied as comonomers for copolymers with SA and they are much more slowly eroding materials. The overall erosion rates of poly(CPH:SA) and poly(CPP:SA) copolymers decrease as the CPH or CPP fraction is increased. These two materials are similar in structure; however, poly(CPH) has a much lower degree of crystallinity.[50] The parameters used for poly(CPH) and poly(CPP) are listed in Table 5. The time step in the poly(CPP) model is 10 s, and the time step in the poly(CPH) model is 50 s.

Table 5. Parameters Used to Model Poly(CPP) and Poly(CPH) Erosion Kinetics

parameter	CPP	CPH
k_{a1}	2.5×10^{-9} (g cm^2 s^{-1})	5.7×10^{-11} (g cm^{-2} s^{-1})
ρ	1.05 (g cm^{-3})	1.05 (g cm^{-3})
k_{d1}	1.4×10^{-8} (cm s^{-1})	1.4×10^{-8} (cm s^{-1})
D_1	7.7×10^{-6} (cm^2 s^{-1})	7.2×10^{-6} (cm^2 s^{-1})
β	0.007	0.001
λ	5.0×10^{-6} (cm)	1.0×10^{-5} (cm)
α	0.62	0.2
y	1.3 (nm)	1.5 (nm)

Table 6. Features of the Erosion for Three Different Homopolymers

polymer	overall erosion rate (mol cm^{-2} s^{-1})	min pH in the erosion zone	erosion zone thickness (μm)
poly(SA)	1.8×10^{-4}	4.8	11.4
poly(CPP)	1.1×10^{-7}	5.2	5.5
poly(CPH)	1.4×10^{-8}	5.6	26.4

For both of these cases, the degradation rate constants were estimated so that the overall erosion rate constant (mass per area per time) would closely match that reported in the literature.[31] The dissolution rate constant for CPH was obtained experimentally as described above and approximated for CPP. The diffusion coefficient for CPP was obtained from Göpferich and Langer[26] and estimated for CPH assuming an inverse dependence of D with respect to molecular weight. The lamellar thickness was estimated for both materials from recent experiments.[45,46] The degree of crystallinity was obtained from the literature.[31]

For both of these materials, an erosion zone forms similar to that formed for poly(SA). In both cases, the porous erosion zone is characterized by saturation of the dissolved dicarboxylic acid and low concentrations of monomer precipitated inside the pores. The major differences among the three homopolymers are the pH inside the erosion zone and the thickness of the erosion zone. These three features are contrasted in Table 6. The differences in the minimum pH are attributed to the properties of the diacids (pK_a and solubility). The differences in the erosion zone thickness are due primarily to differences in the degradation rate constants and, presumably, the degree of crystallinity. Poly(CPP) and poly(SA) have nearly the same degree of crystallinity, but the ratio of the degradation rate constants, β, is larger for poly(CPP). This results in a smaller erosion zone. For poly(CPH), β is the same as that for poly(SA), but the degree of crystallinity is much lower. This permits the erosion front to progress much further into the polymer before the surface begins to move, resulting in a larger erosion zone. The degradation rate constant for poly(CPP) is about 50 times the degradation rate constant for poly(CPH) but there is only about a 10-fold difference in the overall erosion rate. This is because the crystallinity the poly(CPH) is much lower.

Model Solution for Poly(CPH:SA) 20:80

To demonstrate the ability of this model to account for copolymer erosion, we have modeled poly(CPH:SA) 20:80. To estimate the degradation rate constants for CPH in the copolymer, we compare the molar erosion

Table 7. Parameters Used to Model Poly(CPH−SA) 20:80 Erosion Kinetics

parameter	value
k_{a1}	8.0×10^{-7} (g cm^{-2} s^{-1})
k_{a2}	1.3×10^{-10} (g cm^{-2} s^{-1})
ρ	1.05 (g cm^{-3})
k_{d1}	1.4×10^{-6} (cm s^{-1})
k_{d2}	1.4×10^{-8} (cm s^{-1})
D_1	6.8×10^{-6} (cm^2 s^{-1})
D_2	7.2×10^{-6} (cm^2 s^{-1})
β	0.025
δ	2.5×10^{-4}
λ	5.6×10^{-6} (cm)
α	0.467

rate constants for poly(CPH) to that for poly(SA) reported by Leong et al.[51,52] The ratio of the erosion rate constants for poly(SA) to that for poly(CPH) is used as a first approximation for the ratio of degradation rate constants for the SA−SA and CPH−CPH bonds, k_{SA-SA} and $k_{CPH-CPH}$, respectively. We then estimate the degradation rate constant for CPH in the copolymer, k_{CPH}, as

$$2k_{CPH}^{-1} = \frac{(L_{CPH} - 1)k_{CPH-CPH}^{-1} + 2k_{CPH-SA}^{-1}}{1 + L_{CPH}} \quad (23)$$

Here, L_{CPH} is the number average sequence length of CPH in the copolymer reported by Shen et al.[38] and k_{CPH-SA} is the rate constant for the degradation of CPH−SA bonds, approximated here as k_{SA-SA}. The rate constant for degradation of SA−SA bonds is approximated as $2k_{SA}$. The degradation rate constant for SA does not change in the copolymer since k_{SA-SA} is equal to k_{CPH-SA}. This procedure is used to estimate the degradation rate constants for both crystalline and amorphous CPH.

The microphase separation that exists in the copolymer must be accounted for. In this case, we account for the microphase separation by setting the parameter y to 1.5 nm. This is a good approximation for the thickness of a monolayer, as the average monolayer thickness increases when CPH is added. This is also the approximate length scale associated with the microphase separation. Since our model is discretized at this length, the parameters ϕ_{a1} and ϕ_{c1} in eqs 6−9 appropriately account for the microphase separation with a mean field approximation. The crystalline/amorphous phase separation is accounted for by the probabilities in eqs 6−9. The parameters used to model the copolymers are listed in Table 7. The model was solved with a time step of 0.5 s.

It is difficult to fit the copolymer erosion to accurate experimental data for several reasons. First, only a few published results for copolymer erosion report the release of the individual monomers. Those that do report release of the individual monomers have significant uncertainty. This is because it is exceedingly difficult to separate and detect the individual dicarboxylic acids in the release media due to their relative insolubility. The diacids may be assayed by HPLC, but it is difficult to obtain reliable and repeatable results for the aromatic diacid. Therefore, when fitting the model for copolymer erosion to experimental data, we attempted only to match the overall mass loss kinetics and the SA release profile, not the CPH release profile. The overall erosion profile (cumulative fractional mass loss) is shown in Figure 8a for the poly(CPH:SA) 20:80 erosion. Figure 8b shows the individual monomer release profiles for the first 16 h, while the erosion front is developing.

The porosity evolution for the first 10 h is shown in Figure 9. Similar to the poly(SA), a pseudo-steady-state develops, wherein the position of the erosion front (x_{ef}) and the position of the surface (x_s) move through the device with the same velocity. In this case, the erosion zone is about 83 μm thick. We can see in Figure 8b that the release of CPH monomer lags behind the release of SA monomer. This is consistent with our experimental observations and observations made by others of similar copolymer systems.[37,38] The initial delay in the erosion profiles shown in Figure 8 is associated with the time required for the surface of the tablet to approach a porosity of one.

Inside the erosion zone, the composition of the surface can be characterized as it was for the poly(SA). As might be expected, the surface is dominated by crystalline poly(CPH), as this is the most slowly degrading species. About 1.3% of the surface inside the erosion zone is occupied by undissolved CPH monomer. Similar to the homopolymer case, the erosion zone quickly becomes saturated with SA diacid. The pH inside the pores reached the same value as that for the homopolymer until all of the SA was depleted (data not shown). The pH effect limits the solubility of the CPH diacid inside the pores similar to the effect observed for the SA diacid.

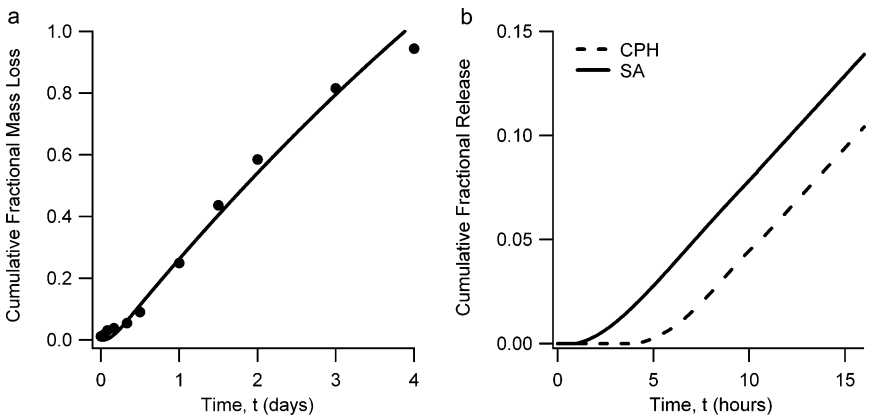

Figure 8. (a) Cumulative fractional mass loss for poly(CPH:SA) 20:80 erosion from experiment[38] (●) and model (line). (b) Cumulative monomer release profiles for the first 16 h for poly(CPH:SA) 20:80.

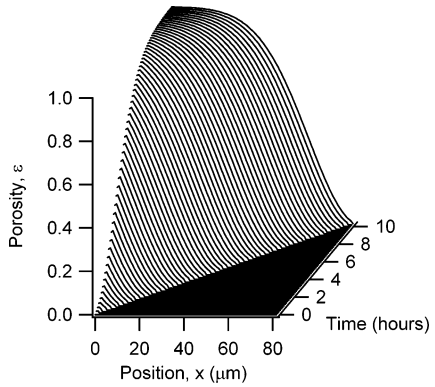

Figure 9. Porosity as a function of time and position for CPH:SA (20:80) copolymer erosion.

Conclusions

The new model for erosion of surface-erodible materials presented here offers the ability to describe many interesting phenomena on a microscopic scale that are difficult to observe directly by experiment. Not only is the erosion kinetics of individual phases discerned, but the information is also resolved at the nanometer length scale. Furthermore, this model can be used to predict phenomena occurring inside the microenvironment of the erosion zone, including concentrations of dissolved monomer species, the resulting pH, and monomer precipitation. A detailed description of the erosion zone will guide the rational design of polyanhydride devices for the delivery of drugs that may be sensitive to pH changes such as vaccines or other therapeutic proteins.

The solutions to the model presented here motivate additional experiments that could describe the erosion process in more detail. Of particular interest are the individual degradation rate constants for crystalline and amorphous moieties and porosity and pH within the eroding zone. Polymer degradation is a stochastic process, and models and experiments for the molecular weight dependence of the degradation constants are needed. Though this model was developed for polyanhydride copolymers, it could be used for a variety of surface- and bulk-eroding systems. Indeed, the results for the copolymer indicate the system is not purely bulk eroding, as the erosion zone represents a significant fraction of the device thickness. Just as the current formulation of the model allows for pH dependence of the dissolution kinetics, pH-dependent polymer degradation could also be accounted for. Further extensions of the model could also account for the release of encapsulated drugs.

For design of drug-loaded systems for controlled-release applications, it is also necessary to have an accurate description of the thermodynamics of the polymer/drug system. Adding a drug may compatibilize the polymer system, affect polymer crystallinity, or form a third phase. Any of these three effects could be dealt with by modifications to this erosion model.

Appendix A.1. Estimation of Probabilities p_{aa} and p_{ca}

In eqs 6−9, the crystalline/amorphous phase separation is accounted for by considering the probability that dissolving monomer exposes amorphous or crystalline polymer. This probability depends on the identity of the monomer element as well. The probabilities are computed by considering the initial volume associated with the interfacial area. This fractional interfacial volume, v_{int}, is computed according to

$$\boldsymbol{v}_{int}(x,t=0) = \frac{\text{Volume of amorphous polymer at interface}}{\text{Volume of polymer}} = \frac{(1-\alpha)\pi d_a y \Delta x}{\left(\frac{\pi d_a{}^2 \Delta x}{4}\right)} = \frac{4(1-\alpha)}{\lambda} \quad \text{(A.1)}$$

Here, d_a is the diameter of an amorphous domain and the volume of amorphous polymer at the interface is the interfacial area multiplied by the thickness of a monolayer, y. The probabilities are then computed as

$$p_{aa} = 1 - \frac{v_{int}}{v_a} \quad \text{(A.2)}$$

$$p_{ca} = \frac{v_{int}}{v_c} \quad \text{(A.3)}$$

Here, v_a and v_c are the volume fractions of the crystalline and amorphous phases, respectively. These are obtained by integrating the dissolution rate of each type of monomer at each time step and are functions of both position and time.

Appendix A.2. Saturation Concentration and pH Calculations

Equation 21 computes the dissolution rate, κ, as a function of the saturation concentration, c_{sat}. The saturation concentration is a strong function of the pH for all of the monomers studied here, as illustrated in Figure 2, and the pH of the microenvironment in the erosion zone is determined by the SA concentration. Five equations are needed to solve for the concentrations of the five species, SA, SA^-, SA^{2-}, H^+, and OH^-. These five equations are the equilibria of SA, SA^-, and water dissociation, the mole balance on the SA derived species, and the charge balance.

$$K_{a1,SA} = \frac{[H^+][SA^-]}{[SA]} \quad \text{(A.4)}$$

$$K_{a2,SA} = \frac{[H^+][SA^{2-}]}{[SA^-]} \quad \text{(A.5)}$$

$$K_w(37\ ^\circ\text{C}) = [H^+][OH^-] = 2.39 \times 10^{-14} \quad \text{(A.6)}$$

$$M_{SA} = [SA] + [SA^-] + [SA^{2-}] \quad \text{(A.7)}$$

$$[H^+] = [SA^-] + 2[SA^{2-}] + [OH] \quad \text{(A.8)}$$

The bracketed variables are molarities of the bracketed species and M_{SA} is the total SA molarity. These five equations can be combined to form a quartic

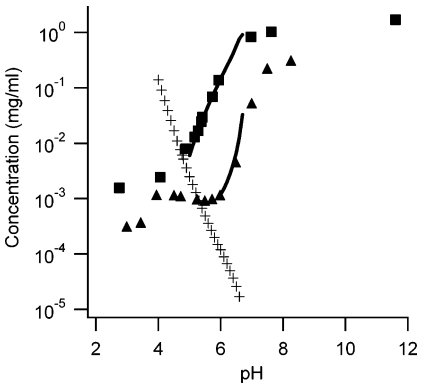

Figure 10. Saturation concentrations of SA (■) and CPH (▲) as a function of pH and concentration of SA that produces the pH according to equation A.9 (+). Solid lines are the model fits, eqs A.10 and A.11 plotted over the ranges that they are used in the model.

equation for $[H^+]$ based on M_{SA}.

$$M_{SA}([H^+]^2 + 2K_{a2,SA}[H^+]) = \frac{1}{K_{a1,SA}}[H^+]^4 + [H^+]^3 + \left(K_{a2,SA} + \frac{K_w}{K_{a1,SA}}\right)[H^+]^2 + K_w[H^+] + K_wK_{a2,SA} \quad (A.9)$$

Most of the terms in this equation over at least a portion of the expected pH range remain if the relatively small terms are neglected. Thus, rather than solving the quartic equation at each x and t for the pH and then predicting c_{sat}, we offer an empirical equation that fits $c_{sat,SA}$ as functions of c_{SA}.

$$\log(c_{sat,SA} - c_{SA}) = -0.252[\log(c_{SA})]^3 - 3.06[\log(c_{SA})]^2 - 12.8\log(c_{SA}) - 1.95 \quad (A.10)$$

A similar approach was used for the other two homopolymers. In the copolymer, we assume that the pH and, hence, the monomer solubility are only a function of the SA concentration since SA is the majority component, degrades and dissolves faster, and has about 10 times the solubility of the CPH. The $c_{sat,CPH}$ was predicted from

$$\log(c_{sat,CPH}) = 0.231c^3 + 3.36c^2 + 14.9c + 17.7$$

$$c = \log(c_{sat,SA}) \quad (A.11)$$

In these equations, all of the concentrations have units of g L^{-1}. These are plotted in Figure 10 along with the saturation data.

The solutions to eqs A.9−A.11 are plotted in Figure 10 along with the saturation data. This plot shows that the minimum pH that can be obtained is about 4.75, as the SA concentration required to obtain lower pH is above the saturation concentration.

References and Notes

(1) Castellanos, I. J.; Cuadrado, W. L.; Griebenow, K. *J. Pharm. Pharmacol.* **2001**, *53*, 1099−1107.
(2) Truong, V. L.; Williams, J. R.; Hildreth, J. E. K.; Leong, K. W. *Drug Delivery* **1995**, *2*, 166−174.
(3) Tamada, J.; Langer, R. *J. Biomater. Sci., Polym. Ed.* **1992**, *3*, 315−353.
(4) Mathiowitz, E.; Saltzman, W. M.; Domb, A.; Dor, P.; Langer, R. *J. Appl. Polym. Sci.* **1988**, *35*, 755−774.
(5) Mathiowitz, E.; Langer, R. *J. Controlled Release* **1987**, *5*, 13−22.
(6) Mathiowitz, E.; Amato, C.; Dor, P.; Langer, R. *Polymer* **1990**, *31*, 547−555.
(7) Chiba, M.; Hanes, J.; Langer, R. *Biomaterials* **1997**, *18*, 893−901.
(8) Thomas, P. A.; Padmaja, T.; Kulkarni, M. G. *J. Controlled Release* **1997**, *43*, 273−281.
(9) Berkland, C.; Kipper, M. J.; Kim, K. K.; Narasimhan, B.; Pack, D. W. *J. Controlled Release* **2004**, *94*, 129−141.
(10) Gross, K. A.; Rodríguez-Lorenzo, L. M. *Biomaterials* **2004**, *25*, 4955−4962.
(11) Guan, J.; Sacks, M. S.; Beckman, E. J.; Wagner, W. R. *Biomaterials* **2004**, *25*, 85−96.
(12) Li, H.; Chen, Y.; Xie, Y. *Mater. Lett.* **2003**, *57*, 2848−2854.
(13) Kipper, M. J.; Shen, E.; Determan, A.; Narasimhan, B. *Biomaterials* **2002**, *23*, 4405−4412.
(14) Chasin, M.; Hollenbeck, G.; Brem, H.; Grossman, S.; Colvin, M.; Langer, R. *Drug Dev. Ind. Pharm.* **1991**, *16*, 2579−2594.
(15) Chasin, M.; Domb, A.; Ron, E.; Mathiowitz, E.; Langer, R.; Leong, K.; Laurencin, C.; Brem, H.; Grossman, S. *Drugs Pharm. Sci.* **1990**, *45*, 43−70.
(16) Jiang, H. L.; Zhu, K. J. *Int. J. Pharm.* **2000**, *194*, 51−60.
(17) Qiu, L. Y.; Zhu, K. J. *Int. J. Pharm.* **2001**, *219*, 151−160.
(18) Fu, J.; Fiegel, J.; Krauland, E.; Hanes, J. *Biomaterials* **2002**, *23*, 4425−4433.
(19) Schwendeman, S. P.; Costantino, H. R.; Gupta, R. K.; Tobio, M.; Chang, C. A.; Alonso, M. J.; Siber, G. R.; Langer, R. In *New Approaches to Stabilization of Vaccines Potency*; Brown, F., Ed.; Karger: Basel, 1996; Vol. 87, pp 293−306.
(20) Zhang, M.; Yang, Z.; Chow, L.-L.; Wang, C.-H. *J. Pham. Sci.* **2003**, *92*, 2040−2056.
(21) Thombre, A. G.; Himmelstein, K. J. *Biomaterials* **1984**, *5*, 249−254.
(22) Thombre, A. G.; Himmelstein, K. J. *AIChE J.* **1985**, *31*, 759−766.
(23) Zygourakis, K. *Chem. Eng. Sci.* **1990**, *45*, 3259−2366.
(24) Zygourakis, K.; Markenscoff, P. A. *Biomaterials* **1996**, *17*, 125−135.
(25) Goepferich, A.; Langer, R. *Macromolecules* **1993**, *26*, 4105−4112.
(26) Goepferich, A.; Langer, R. *J. Controlled Release* **1995**, *33*, 55−69.
(27) Batycky, R. P.; Hanes, J.; Langer, R.; Edwards, D. *J. Pharm. Sci.* **1997**, *86*, 1464−1477.
(28) Varelas, C. G.; Dixon, D. G.; Steiner, C. A. *AIChE J.* **1995**, *41*, 805−811.
(29) Varelas, C. G.; Dixon, D. G.; Steiner, C. A. *J. Controlled Release* **1995**, *34*, 185−192.
(30) Larobina, D.; Kipper, M. J.; Mensitieri, G.; Narasimhan, B. *AIChE J.* **2002**, *48*, 2960−2970.
(31) Narasimhan, B.; Kipper, M. J. *Adv. Chem. Eng.* **2004**, *29*, 169−218.
(32) Mathiowitz, E.; Jacob, J.; Pekarek, K.; Chickering, D. I. *Macromolecules* **1993**, *26*, 6756−6765.
(33) Shakesheff, K. M.; Davies, M. C.; Roberts, C. J.; Tendler, S. J. B.; Shard, A. G.; Domb, A. *Langmuir* **1994**, *10*, 4417−4419.
(34) Shakesheff, K. M.; Davies, M. C.; Domb, A.; Jackson, D. E.; Roberts, C. J.; Tendler, S. J. B.; Williams, P. M. *Macromolecules* **1995**, *28*, 1108−1114.
(35) Heatley, F.; Humadi, M.; Law, R. V.; D'Emanuele, A. *Macromolecules* **1998**, *31*, 3832−3838.
(36) McCann, D. L.; Heatley, F.; D'Emanuele, A. *Polymer* **1999**, *40*, 2151−2162.
(37) Tamada, J. A.; Langer, R. S. *Proc. Int. Symp. Controlled Release Bioact. Mater.* **1990**, *17*, 156−157.
(38) Shen, E.; Kipper, M. J.; Dziadul, B.; Lim, M.-K.; Narasimhan, B. *J. Controlled Release* **2002**, *82*, 115−125.
(39) Goepferich, A.; Langer, R. *J. Polym. Sci., Part A: Polym. Chem.* **1993**, *31*, 2445−2458.
(40) Goepferich, A.; Schedl, L.; Langer, R. *Polymer* **1996**, *37*, 3861−3869.
(41) Mäder, K.; Nitschke, S.; Stosser, R.; Borchert, H.-H.; Domb, A. *Polymer* **1997**, *38*, 4785−4794.
(42) Park, E.-S.; Maniar, M.; Shah, J. *J. Controlled Release* **1996**, *40*, 111−121.
(43) Santos, C. A.; Freedman, B. D.; Leach, K. J.; Press, D. L.; Scarpulla, M.; Mathiowitz, E. *J. Controlled Release* **1999**, *60*, 11−22.
(44) Kipper, M. J.; Seifert, S.; Thiyagarajan, P.; Narasimhan, B. *Polymer* **2004**, *45*, 3329−3340.
(45) Kipper, M. J.; Seifert, S.; Thiyagarajan, P.; Narasimhan, B. *J. Polym. Sci., Part B: Polym. Phys.* **2005**, *43*, 463−477.

(46) Shen, E.; Pizsczek, R.; Dziadul, B.; Narasimhan, B. *Biomaterials* **2001**, *22*, 201−210.
(47) Shen, E. E.; Chen, H.-L.; Narasimhan, B. *Proc. Mater. Res. Soc.* **2001**, *662*, N. N.4.2.1-N. N.4.2.5.
(48) D'Emanuele, A.; Hill, J.; Tamada, J. A.; Domb, A. J.; Langer, R. *Pharm. Res.* **1992**, *9*, 1279−1283.
(49) Hoffman, J. D. *Numerical Methods for Engineers and Scientists*; McGraw-Hill, Inc.: New York, 1992.
(50) Mathiowitz, E.; Ron, E.; Mathiowitz, G.; Amato, C.; Langer, R. *Macromolecules* **1990**, *23*, 3212−3218.
(51) Leong, K.; Simonte, V.; Langer, R. *Macromolecules* **1987**, *20*, 705−712.
(52) Leong, K. W.; Brott, B. C.; Langer, R. *J. Biomed. Mater. Res.* **1985**, *19*, 941−955.

MA047661R